# Effect of Polar Surfaces on Decomposition of Molecular Materials

Maija M. Kuklja,* Roman V. Tsyshevsky, and Onise Sharia

Materials Science and Engineering Department, University of Maryland, College Park, Maryland 20742, United States

S *Supporting Information*

ABSTRACT: We report polar instability in molecular materials. Polarization-induced explosive decomposition in molecular crystals is explored with an illustrative example of two crystalline polymorphs of HMX, an important energetic material. We establish that the presence of a polar surface in δ-HMX has fundamental implications for material stability and overall chemical behavior. A comparative quantum-chemical analysis of major decomposition mechanisms in polar δ-HMX and nonpolar β-HMX discovered a dramatic difference in dominating dissociation reactions, activation barriers, and reaction rates. The presence of charge on the polar δ-HMX surface alters chemical mechanisms and effectively triggers decomposition simultaneously through several channels with significantly reduced activation barriers. This results in much faster decomposition chemistry and in higher chemical reactivity of δ-HMX phase relatively to β-HMX phase. We predict decomposition mechanisms and their activation barriers in condensed δ-HMX phase, sensitivity of which happens to be comparable to primary explosives. We suggest that the observed trend among polymorphs is a manifestation of polar instability phenomena, and hence similar processes are likely to take place in all polar molecular crystals.
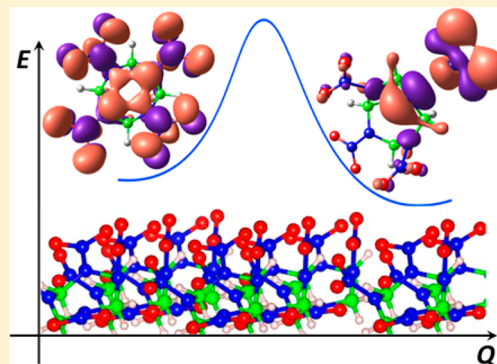
1. INTRODUCTION

The earliest stages of fast decomposition chemistry of energetic materials continue keeping their secrets.[1−4] Researchers still struggle with the understanding of how a modest amount of external energy[5,6] insufficient to break a single chemical bond in a molecule[7−9] is able to start a violent explosive chemical reaction and release substantial thermal energy stored in energetic materials.[10,11]

A chemical reaction of decomposition can start from the ground state of the system or from one of its excited vibrational or/and electronic states.[12,13] Various mechanisms of initiation of the decomposition chemistry and further processes leading to products have been discussed over the years. For example, electronic transport,[14] a multiprocess photochemical model,[15,16] and an excitonic mechanism[7,8] were proposed as possible means of detonation initiation. Despite abundant experimental evidence that electronic excitations (electrons, holes, and excitons) play an important role in the initiation of chemistry in energetic materials,[17−26] the details of processes involving electronic excitations are far from being understood. Once the electronic structure calculations of ideal energetic materials[27,28] were initiated and simple defects in them[29−31] were simulated, a great deal of knowledge became available.[32] Despite this, even a general concept of electronic excitations being able to trigger explosive decomposition chemistry is not broadly accepted in the field of energetic materials (see, for example, discussions in refs 8, 13, 18, 26, and 33). This is particularly disheartening because photochemistry of organic molecules is a well-established field of science with many good textbooks.

A scrupulous *ab initio* study that methodically analyzed and compared energies of decomposition reactions on ground and excited potential energy surfaces was performed for 2,2-dinitroethene-1,1-diamine (DADNE, see Figure 1 in Supporting Information) molecules.[34] This research established that a dramatic effect of charged states on decomposition chemistry is manifested in reduced activation barriers, an altered dominating chemistry mechanism, and pronounced exothermicity of reactions. Consistent conclusions were obtained in recent experimental studies in which laser irradiation was used to initiate decomposition of other energetic materials, 1,3,5-trinitroperhydro-1,3,5-triazine (RDX),[25] pentaerythritol tetranitrate (PETN),[18,26,35] and heterocyclic molecules.[36,37] The laser-induced decomposition of nitramines, nitroesters, and nitro heterocycles suggests that excitations at 260−190 nm yield the initial product of NO, appearing in <100 fs, showing ultrafast kinetics.[13] The ground-state thermal decomposition would rather produce NO_2 as an initial product.[11,38−41]

The use of laser initiation brings about a possibility of precise control of the explosive decomposition chemistry in energetic materials once we establish details of the interplay of molecular interactions and materials' response to an external perturbation. The method for generating charged (or excited) states in *molecules* (particles) under laser excitation seems straightforward, whereas mechanisms for appearance of charged and/or excited states (quasi-particles) in energetic *crystals* (and
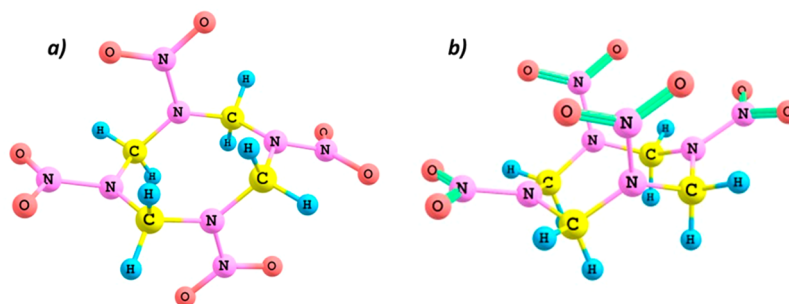
Figure 1. Molecular structures of (a) a chair β-HMX conformer and (b) a boat δ-HMX conformer.

broader, molecular materials) have yet to be elucidated.[8,18,23,25,33]

In this study, we explore an outstanding fundamental challenge of surface chemistry on a polar molecular material. On one hand, accelerated surface chemistry was reported for polar molecular crystals, for example, in the reaction with ammonia of *p*-chlorobenzoic anhydride.[42,43] A puzzling difference in the anisotropy of the reactions was suggested wherein the nonpolar chloro anhydride undergoes reaction at approximately the same rate in any direction parallel to the major face of the crystal, however the polar bromo anhydride reacts much faster along the polar axis than along those directions normal to it. Despite tremendous advances in the science of molecular crystals, including virtuoso synthesis, sophisticated characterization, and stunningly wide range of applications, detailed microscale mechanisms of such accelerated chemical reactions remain unclear. On the other hand, the question of surface polarity in ion-covalent crystals has a long history and several alternative polarity compensation mechanisms were discussed.[44] The presence of a macroscopic surface dipole in ionic crystals is known to produce an electrostatic instability, which can be canceled by compensating charges in the outer planes. This can be achieved either by a deep modification of the surface electronic structure, full or partial filling of surface states, sometimes leading to surface metallization, or by strong changes in the surface stoichiometry, spontaneous desorption of atoms, faceting, large-cell reconstructions due to the ordering of surface vacancies, etc.[45,46]

A polarization instability, the phenomenon similar to what is observed in ion-covalent oxides, has never been reported in organic materials. Here we discover that a polar surface triggers a fast chemical decomposition of the molecular material due to a polarized surface charge. We perform quantum-chemical calculations of decomposition pathways of two octahydro-1,3,5,7-tetranitro-1,3,5,7-tetrazocine ($C_4N_8H_8O_8$, also known as HMX or octogen) polymorphs. Similar to other molecular crystals, in which polar and nonpolar polymorphs were noted to behave differently, HMX decomposition has been studied over dozens of years, but the problem of why different polymorphs of the same stoichiometry exhibit visibly different chemical reactivity remains unanswered.[47] Our modeling offers a possible resolution for the stubborn problem of sensitivity to detonation and suggests new insight on many seemingly contradictory experimental data. We explain how the (001) surface of polar δ-HMX induces a separation of positive and negative charges, creating conditions that trigger the explosive decomposition chemistry, while nonpolar β-HMX does not exhibit this kind of behavior. We predict decomposition mechanisms and activation barriers of δ-HMX. With the conclusions obtained on the vivid illustrative example of HMX,

we propose that other molecular materials in different polymorphs will have similar behavior. This forecast offers a strategy to analyze materials reactivity based on polymorph's structure and composition; it opens up vast new opportunities in materials design and unprecedented control of surface chemistry.

2. HMX AS A MODEL SYSTEM

HMX is one of the most important solid energetic materials with multiple applications ranging from high-explosives and propellants to rocket and space shuttle engine fuels. There are four known crystal phases of HMX usually labeled α,[48] β,[49] γ,[50] and δ.[51] Monoclinic β-HMX, the most stable under ambient conditions phase, has $P2_1/c$ ($P2_1/n$) symmetry and two molecules per unit cell.[49] When heated to ~160 °C, β-HMX converts to the most reactive hexagonal δ-phase[51−56] with $P6_1$ symmetry and six molecules per unit cell.[51] While the phase transition is reversible, depending on sample purity and crystallinity, it takes hours or even weeks for δ-HMX to convert back to β-HMX at room temperature.[52] In addition, it was noted that facets of β-HMX single crystals often contain deposits of δ-HMX, with size and concentration strongly dependent on the synthesis conditions.[57] The δ-phase exhibits much higher sensitivity to detonation initiation than the β-phase, and significant differences between the two phases were also noted in burn rates and drop height measurement experiments.[58,59] It was speculated that the observed sensitivity increase of the δ-phase is due to a density reduction from 1.90 of the β-phase to 1.79 g/cm³ of the δ-phase and the corresponding lattice expansion that accompanies the β-to-δ phase transition, which results in an appearance of cracks, large amounts of hot spots in the material, and the fast growth of reaction during shock compression.[60] The modification of the molecular structure from β-HMX chair (Figure 1a) to δ-HMX boat configuration (Figure 1b) was also suggested to affect sensitivity of HMX polymorphs due to changed intra- and intermolecular interactions.[61]

Typically, energetic and kinetic parameters of decomposition of energetic materials are somewhat scattered because several dissociation processes coexist and only global kinetics is experimentally measured. However, activation energies of overall thermal decomposition of condensed HMX are scattered in an unusually wide range, from 13 to 67 kcal/mol, with appreciably narrower intervals assigned to decomposition in melt (47.1−64.7 kcal/mol) and in the gas phase (32.1−52.9 kcal/mol).[62] Judging by the described conditions of experiments, these data are mostly relevant to the β-HMX phase.[62] On the other hand, theoretical studies show that the decomposition of β-HMX in gas phase[38,63] and solid

13290

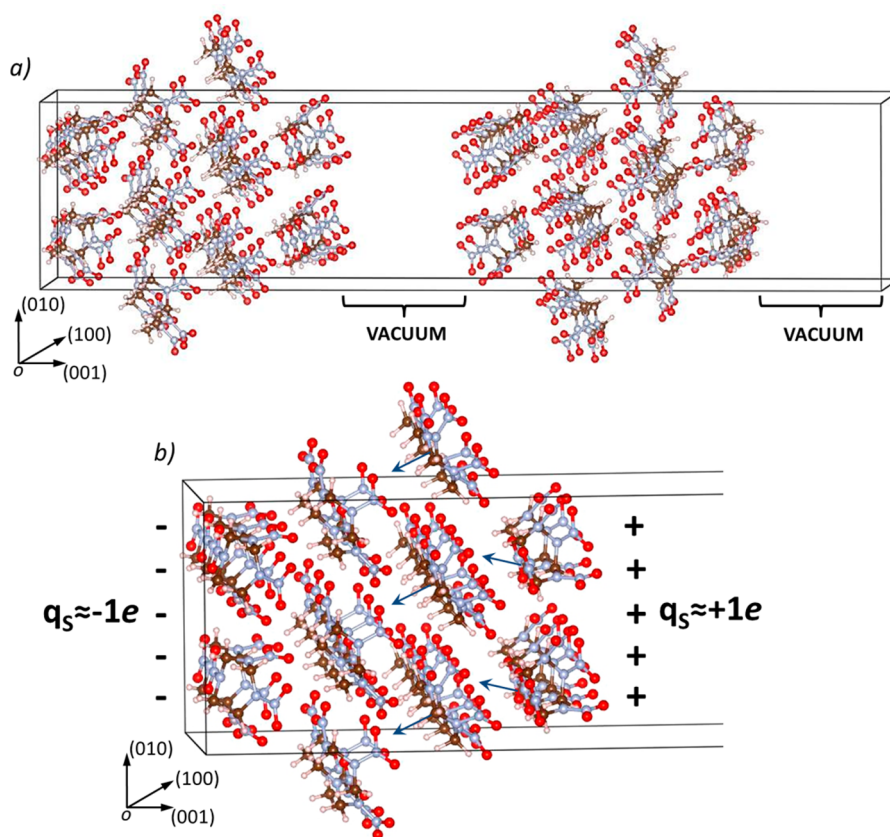dx.doi.org/10.1021/ja506297e | *J. Am. Chem. Soc.* 2014, 136, 13289−13302

Figure 2. (a) A slab model of (001) surface of δ-HMX supercell containing 32 molecules, with the lattice parameters of a = 16.360 Å, b = 14.168 Å, c = 63.789 Å, $\alpha = \beta = \gamma = 90°$. (b) A fragment of the supercell illustrates the dipole-induced charge polarization; q_s stands for the surface charge, and blue arrows schematically represent directions of molecular dipole moments.

state[11,39,40] requires 40−46 kcal/mol in energy. Undoubtedly, the decomposition of condensed HMX is a complex process, which strongly depends on conditions of experiment and hence calls for a careful explanation. Recent DSC and TGA measurements[64] of the HMX decomposition performed on polymer-bonded explosive PBXN-9 containing 92% of HMX suggested that the activation barrier, E_a, ranges from 33.7 to 46.6 kcal/mol and pre-exponential factor lgA falls in the interval from 11 to 17 (s^{-1}). Some authors suggest that the decomposition is accompanied or preceded by the β-HMX $\rightarrow$ δ-HMX transition,[52,54] although the exact amount of material that decomposes from one or the other phase probably depends on the heating rate.[47,65]

Experimental measurements of δ-HMX thermal decomposition are largely lacking with an exception of two studies[66,67] that reported the activation barrier of 34.4 kcal/mol and the pre-exponential factor of lgA = 15.3 (s^{-1}).

Apparent coincidence of energy barriers obtained for β- and δ-HMX in some studies that is in a sharp contrast with large scattering of data registered in other studies emphasizes quite a few questions regarding a detailed mechanism and the consequence of steps of the HMX decomposition. For example, what drives rapid decomposition of the highly explosive δ-phase in comparison to the more stable β-phase? Answers to these questions would significantly advance our understanding of the relationship between the chemical decomposition and stability/degradation processes, molecular and crystalline polymorphism, and morphology of crystals. Such an understanding will go well beyond providing a consistent interpretation of existing experiments and will also allow us to design further

experimental studies and make important inroads into constructing a microscopic theory of sensitivity to detonation initiation.

3. DETAILS OF CALCULATIONS

Our calculations were performed using a combination of density functional theory (DFT),[68,69] variational transition-state theory (TST), and *ab initio* chemical kinetics, with large-scale quantum-chemical molecular and periodic solid-state calculations of ideal and defect containing materials.

Chemical reactions in the gas phase were modeled using DFT in the GGA approximation with the PBE functional,[70] hybrid exchange correlation-corrected PBE0 functional,[71] and dispersion-corrected wB97XD functional[72] as implemented in the molecular GAUSSIAN code.[73] The PBE functional was further used for investigating solid-state reaction mechanisms. Hence the initially performed PBE molecular calculations were compared to these carried out using the hybrid PBE0 and dispersion-corrected wB97XD functionals for additional validation. Unlike PBE, both PBE0 and wB97XD functionals consume significant CPU time and computer resources but are usually considered relatively reliable for modeling reactions in the gaseous phase (see, for example, ref 74). The electronic structure and decomposition pathways of molecular ions of δ-HMX were modeled using PBE and the hybrid M06[75] functional. All molecular calculations were performed using the split-valence double-ζ 6-31+G(2df,p) basis set. Vibrational frequencies were calculated for relevant atomistic configurations to distinguish energy minima and transition states and to

determine corresponding zero-point energy (ZPE) corrections. The stationary points corresponding to the energy minimum were positively identified by having no imaginary frequencies, and the transition states had exactly one imaginary frequency.

Periodic solid-state calculations were performed using the GGA PBE functional and PAW pseudopotentials[76] as implemented in the plane wave VASP code.[77−79] The kinetic energy cutoff was set to 600 eV. Surface reactions were simulated by using a slab model containing two symmetric lattice fragments each consisting of four-molecule-thick (001) surface layers on top of 10 Å of vacuum (Figure 2). One fragment in the slab is a mirror reflection of the other fragment. Such a 32-molecule (896-atom) supercell with zero total dipole moment was purposely built to remove an artificial electric field in the vacuum layer, which affects the energies of the bond breaking reactions and may lead to overestimated activation barriers.[80]

Minimal energy paths in VASP periodic calculations were obtained with the nudged elastic band method.[81] In the case of GAUSSIAN molecular calculations, an intrinsic reaction coordinate analysis was carried out by using the Hessian-based predictor-corrector integrator algorithm[82,83] for each transition state. Pre-exponential factors were calculated with conventional TST[84] for the decomposition reactions that proceed through a formation of a transition state and with variational TST[85] for the homolytic cleavage pathways, as detailed elsewhere.[38] Bader charges were analyzed by using Bader charge analysis code.[86−88]

4. MODELING DECOMPOSITION MECHANISMS

The main products of thermal decomposition of HMX at ambient and low pressure are CH_2O, N_2O, HCN, HONO, and NO_2. As the heating rate and temperature increase, HCN and NO_2 dominate, and CH_2O and N_2O play a lesser role.[89]

4.1. Gas-Phase Chemical Reactions. The thermal decomposition of gas-phase δ-HMX molecules was explored by simulating five plausible mechanisms, schematically illustrated in Figure 3. Those include: (1) a homolytic cleavage
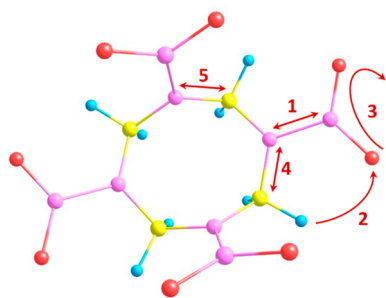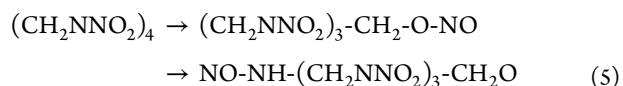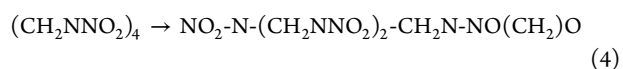
Figure 3. Schematic representation of δ-HMX thermal decomposition pathways.

of the N−NO_2 bond (eq 1), (2) an elimination of the nitrous acid (HONO, eq 2), (3) a nitro−nitrite isomerization (NONO, eq 3), (4) a homolysis of the axial C−N bond in the ring (a-C−N), (eq 4), and (5) a two-step ring opening (eq 5), which proceeds through an isomerization of the δ-HMX molecule into a 10-member oxy-ring structure and its subsequent opening via the C−O bond fission. The three former mechanisms were studied for both axial and equatorial nitro groups. Structures of reaction products and transition-state

configurations are provided in Supporting Information. The reaction (eq 1) proceeds with no barrier.

$$(CH_2N\text{-}NO_2)_4 \rightarrow (CH_2N\text{-}NO_2)_3\text{-}CH_2N^\bullet + {}^\bullet NO_2 \quad (1)$$

$$(CH_2N\text{-}NO_2)_4 \rightarrow (CH_2N\text{-}NO_2)_3\text{-}CHN + HONO \quad (2)$$

$$(CH_2N\text{-}NO_2)_4 \rightarrow (CH_2N\text{-}NO_2)_3\text{-}CH_2N\text{-}ONO \quad (3)$$

$$(CH_2NNO_2)_4 \rightarrow NO_2\text{-}N\text{-}(CH_2NNO_2)_2\text{-}CH_2N\text{-}NO(CH_2)O \quad (4)$$

$$(CH_2NNO_2)_4 \rightarrow (CH_2NNO_2)_3\text{-}CH_2\text{-}O\text{-}NO$$
$$\rightarrow NO\text{-}NH\text{-}(CH_2NNO_2)_3\text{-}CH_2O \quad (5)$$

4.1.1. N−NO₂ Homolysis. A homolytic detachment of a nitro group (eq 1) is usually considered the primary decomposition step in nitro explosive compounds. Table 1 shows that all employed quantum chemistry methods, PBE, PBE0, and wB97XD, produced close activation energies of both axial and equatorial homolytic N−NO_2 bond cleavage processes with the equatorial bond requiring a slightly higher energy (by ∼2 kcal/mol) than the axial bond. The calculated energies (40.3−46.2 kcal/mol, Table 1) are somewhat higher than the experimental energy reported for δ-HMX (34.4 kcal/mol).[66] Energies of the N−N bond cleavage, calculated using different DFT functionals (Table 1), were found in good agreement with recent B3LYP/6-31G(d) estimates of 45.4 and 45.6 kcal/mol, reported for the axial and equatorial N−N bonds of δ-HMX, respectively.[63] Calculated reaction rates depicted in Figure 4 and pre-exponential factors (Table 1) show that the homolytic cleavage of N−N bond in δ-HMX is the predominant decomposition pathway.

4.1.2. HONO Elimination. The concerted HONO elimination mechanism (eq 2) usually requires a slightly higher energy as compared to the homolytic NO_2 loss in different classes of nitro compounds and is often considered a competing mechanism. We note here that the formation of HONO isomers is not observed in δ-HMX. Instead, the molecular relaxation due to a hydrogen transfer causes the HONO moiety to split away without forming an isomer. The activation barriers of axial and equatorial HONO elimination, calculated using hybrid PBE0 and wB97XD functionals, are ∼2−5 kcal/mol higher than the N−N bond dissociation energy (Table 1), with the axial HONO being slightly energetically more favorable than the equatorial HONO. PBE underestimates activation barriers for HONO elimination (∼10−15 kcal/mol) relative to PBE0 and wB97XD predictions (Table 1), which is a well-known trend of pure DFT methods to underpredict the activation barriers for proton migration reactions versus data yield by hybrid functionals.[41,90,91] PBE overestimates bond lengths in the transition-state structures as compared to hybrid PBE0. At the same time, the bond lengths and valence angles of reagents and final products calculated with all three PBE, PBE0, and wB97XD approximations were found in good agreement with each other, which explains close correspondence in reaction energies collected in Table 1. All methods predict the axial HONO elimination to be a weakly exothermic reaction, in contrast to the endothermic elimination of equatorial HONO (∼14 kcal/mol, Table 1). The HONO elimination proceeds at lower rates than the N−N bond cleavage (Figure 4) owing to noticeably lower pre-exponential factors (Table 1).

4.1.3. NONO Rearrangement. The NONO rearrangement (eq 3) proceeds via a pseudo rotation of the nitro group,

Table 1. Calculated Activation Barriers (E, kcal/mol), Zero-Point Energy Corrected Barriers (E_{ZPE}, kcal/mol), Reaction Energies (given in parentheses), and Pre-Exponential Factors (lgA, s^{-1}) of δ-HMX Decomposition Reactions

	reaction	PBE			PBE0			wB97XD		
		E	E_{ZPE}	lgA	E	E_{ZPE}	lgA	E	E_{ZPE}	lgA
1	a-NO$_2$ loss	45.1	40.3	18.4	46.4	41.5	18.4	47.7	43.2	17.9
	e-NO$_2$ loss	46.3	42.0	17.6	48.2	43.8	17.7	50.5	46.2	17.7
2	a-HONO	38.0 (0.7)	33.3 (−2.9)	13.3	48.6 (3.6)	44.1 (0.0)	13.1	51.3 (2.4)	47.1 (−1.2)	12.9
	e-HONO	41.5 (14.5)	36.8 (10.8)	13.4	52.2 (17.9)	47.6 (14.1)	13.4	55.9 (17.7)	51.2 (14.0)	13.7
3	a-NONO	71.3 (20.7)	67.3 (19.1)	15.4	88.8 (23.8)	85.3 (22.2)	14.3	90.6 (21.8)	87.3 (20.6)	14.3
	e-NONO	67.3 (19.6)	53.2 (18.1)	15.1	79.9 (23.6)	75.8 (21.9)	14.8	85.3 (20.8)	81.4 (19.6)	14.6
4	axial C−N ring homolysis	50.0 (49.4)	48.2 (47.7)	12.9	55.9 (54.6)	54.4 (53.4)	12.9	57.5 (55.4)	46.3 (54.5)	13.0
5	oxy-ring isomer formation	47.3 (12.9)	44.8 (12.8)	13.4	56.6 (14.4)	54.3 (14.5)	13.4	57.6 (15.0)	55.5 (15.3)	13.4
	opening of oxy-ring	28.5 (−13.3)	23.9 (−16.1)	−	40.4 (−11.7)	35.6 (−14.5)	−	43.2 (−16.0)	38.6 (−18.5)	−
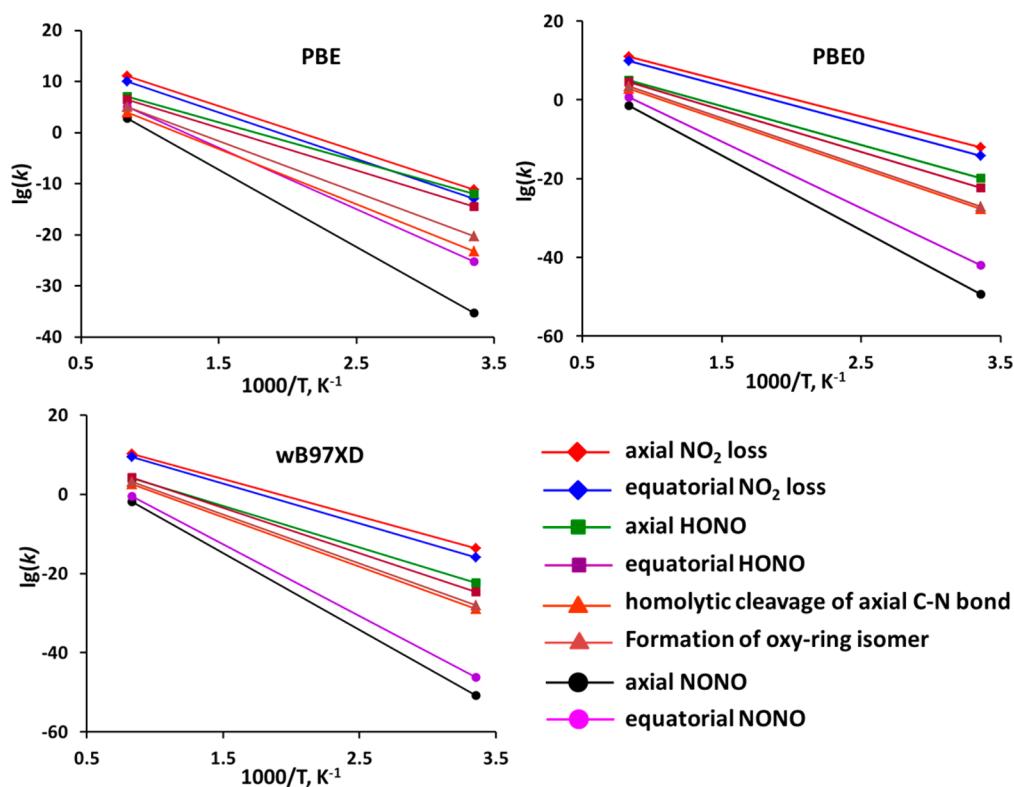
Figure 4. Reaction rates of gas-phase decomposition reactions of δ-HMX.

yielding nitrite isomers, and can be considered as a primary step of a consequent loss of nitric oxide. Recent combined experimental and theoretical decomposition studies suggested that the NONO rearrangement is the primary decomposition step of electronically excited nitro explosives and their model molecules[13] followed by the formation of nitric oxide.

Our calculations revealed that the NONO rearrangement requires high activation barriers (Table 1). An analysis of geometry parameters of transition-state structures (see Supporting Information) shows that PBE overestimates the N8−N1 and the N8−O7 interatomic distances as compared to hybrid PBE0. As a result, PBE underestimates the activation barrier (by ∼20 kcal/mol) relative to hybrid functionals. A similar trend has been also observed in our recent calculations of heterocyclic furazan-based derivatives BNFFs.[92] Both the equatorial and axial NONO rearrangement reactions are highly endothermic. The axial and equatorial nitrite isomers of δ-HMX were found to lie higher in energy than δ-HMX molecule by ∼20 kcal/mol. The high activation barriers rule out the

NONO reaction as a candidate initiation pathway (Figure 4), despite of the relatively high pre-exponential factors (Table 1).

4.1.4. Homolysis of the Axial C−N Bond of the Ring. We explored two possible pathways of HMX ring opening. The first possible channel (eq 4, Figure 3) proceeds via a cleavage of the C4−N3 bond accompanied by a cyclization of the C4N5N6O6 fragment into a four-member oxy-ring, similarly to a mechanism proposed earlier for β-HMX.[63] Table 1 indicates that the activation barrier predicted by PBE0 is almost 15 kcal/mol higher than the N−N bond dissociation energy (Table 1), whereas the activation barrier obtained from wB97XD is only 3 kcal/mol higher than the energy of the axial N−N bond cleavage and practically coincides with the energy required for the equatorial N−N bond fission. We note that ZPE corrections have a large effect (∼11 kcal/mol) on the wB97XD-calculated activation barrier. In contrast to the HONO and NONO reactions, pure PBE produces the activation barriers that are relatively close to PBE0 and wB97XD values. An analysis of the transition-state structures

Table 2. Ionization Potentials (IP, eV) and Electron Affinities (EA, eV) Are Calculated with M06 (and PBE) Functionals for Vertical (v) and Adiabatic (ad) Processes

molecule	IP_v	IP_{ad}	EA_v	EA_{ad}
NO_2	11.49 (11.26)	9.50 (9.49)	1.36 (1.22)	2.26 (1.98)
NO_2 (exp)	11.23[a]	9.60[b]	–	2.27[c]
δ-HMX	10.58 (9.49)	10.10 (9.24)	0.78 (1.24)	1.42 (1.67)
$(CH_2N\text{-}NO_2)_3\text{-}CH_2N$	10.00 (9.13)	7.08 (6.72)	2.21 (2.21)	2.89 (3.24)

[a]From ref 102. [b]From ref 103. [c]From ref 104.

indicates that discrepancies in bond distances predicted at PBE and PBE0 levels are significantly smaller if compared to the HONO and NONO decomposition pathways.

The calculated reaction rates plotted in Figure 4 indicate that the homolytic cleavage of the C−N ring bond is unlikely to compete with the N−N bond cleavage during gas-phase decomposition due to a relatively high activation barrier and low pre-exponential factor (Table 1).

4.1.5. Formation and Opening of the Oxy-Ring Isomer. Another possible path of the HMX ring opening (eq 5, Figure 3) proceeds in two steps. The primary step involves a formation of the 10-member oxy-ring isomer of δ-HMX accompanied by the equatorial C3−N2 bond breaking and the formation of the C3−O2 bond. According to our calculations using hybrid functionals, the formation of the 10-member oxy-ring isomer requires the same amount of energy as the HMX ring opening via homolysis of the C−N ring bond, though PBE functional underestimates the activation barrier by ∼13 kcal/mol (Table 1). Opening of the oxy-ring isomer proceeds via breaking the N4−O2 bond and the H5 hydrogen migration from C3 carbon to N2 nitrogen. The secondary ring opening step requires a significantly lower energy (∼20 kcal/mol, Table 1) than the isomerization step. The HMX ring opening via the oxy-ring isomer formation is a highly exothermic reaction generating heat of ∼16 kcal/mol (Table 1). Nevertheless, the noticeably high activation energy and low pre-exponential factors obtained for this stepwise rearrangement channel do not allow us to consider this pathway as a feasible initiation mechanism to be able to compete with the N−N bond cleavage and HONO elimination channels.

4.1.6. Comparing Molecular Conformers of HMX. A careful comparison of the results described in several DFT studies of the gas-phase decomposition of α-,[93] β-[38,63] and δ- HMX conformers,[63,80] including the current work, leads us to conclude that the modifications of the HMX molecular structure from the boat to the chair configurations do not crucially affect the N−NO$_2$ bond strength and the activation barrier of the HONO elimination in the gas-phase decomposition of the ground state molecules. Hence, these conclusions suggest that intramolecular interactions play a minor role in the sensitivity of materials to detonation. The chemical composition and the presence of chemical functional groups (such as nitro group, amino group etc.) are important factors, but mutual positions of those groups relative to each other are of a significantly lesser importance as illustrated in this example. Therefore, the difference in sensitivities of the β- and δ-HMX phases cannot be explained on the basis of intramolecular interactions contrary to earlier predictions.[61] Extrapolating to other explosive materials, we reiterate[32,34] that while molecular calculations give valuable insight on decomposition mechanisms in the gas phase, it is inappropriate to speculate about the sensitivity to detonation initiation of materials (and even chemical reactivity in general) by using

results of molecular modeling alone. Solid-state simulations are critical in advancing our understanding of microscale mechanisms of sensitivity.

4.2. Molecular Ions. Previously, it was discovered that the decomposition of charged or electronically excited nitro molecules (e.g., DADNE) requires significantly lower activation energies and may trigger different chemical pathways than those available for neutral molecules.[34] Those results lent strong support to the excitonic mechanism of initiation of chemistry in explosives proposed earlier.[7,8] The predictions and conclusions[34] are consistent with recent experimental studies in which laser irradiation was used to initiate decomposition of secondary explosives, RDX,[25] PETN,[18,26,35] heterocyclic molecules,[36,37] functionalized tetrazines,[94] and metal perchlorates.[95] In this section, we explore the effect of charged states on the molecular decomposition of δ-HMX to see if charge transfer (or charge trapping) is able to shed some light on the difference in sensitivity of HMX polymorphs.

Prior to modeling the decomposition reactions of charged ion radicals, we simulated the charging process and obtained ionization potentials and electronic affinities for reagents and reaction products. The obtained energy for removal of an electron (11.49 eV) from an NO$_2$ molecule is very close to the experimental measurement of 11.23 eV (Table 2). The same is true for the corresponding adiabatic process (9.49 vs 9.59 eV) and for trapping an electron (2.26 vs 2.27 eV, Table 2) on NO$_2$. We also note here that energies obtained with PBE functional are consistently close to the M06 and experimental results. Apparent agreement of the calculated and experimental energies serves as a good indication of quality of these calculations and suggests that charging of HMX and $(CH_2N\text{-}NO_2)_3\text{-}CH_2N$ will be simulated with sufficient accuracy, which is imperative for reliable simulations of decomposition of ions.

The calculated vertical ionization potential (IP_{vert}) of δ-HMX is 10.58 eV (Table 2), consistent with IPs of a series of relevant molecules, for example, a nitromethane molecule, CH$_3$NO$_2$, a simple prototype of nitro molecules (11.16 eV[34] and 11.07 ± 0.04 eV[96]), dimethylnitramine (9.53),[97,98] DADNE (9.52 eV),[34] nitroethane (10.91−11.02 eV),[99,100] and tetranitromethane (12.55 eV).[98,101]

The relaxation energy in the equilibrium configuration of δ-HMX$^{\bullet+}$, corresponding to the difference between IP_{vert} and the adiabatic ionization potential (IP_{ad}), is 0.48 eV (11.1 kcal/mol, Table 2). The corresponding relaxation energies of NO$_2$ (>2 eV) and $(CH_2N\text{-}NO_2)_3\text{-}CH_2N$ (>3 eV) are considerably larger than that of δ-HMX$^{\bullet+}$. The large relaxation energy points to the existence of well-localized holes in the system. We observe that out of the three molecules, $(CH_2N\text{-}NO_2)_3\text{-}CH_2N$ has the lowest IP and the highest EA. This implies that any additional charge will likely be localized on $(CH_2N\text{-}NO_2)_3\text{-}CH_2N$ rather than on NO$_2$ in the course of the bond dissociation.

4.2.1. Decomposition of δ-HMX$^{\bullet+}$. An ionized molecule of δ-HMX (hereafter referred to as δ-HMX$^{\bullet+}$) has C$_2$ symmetry.
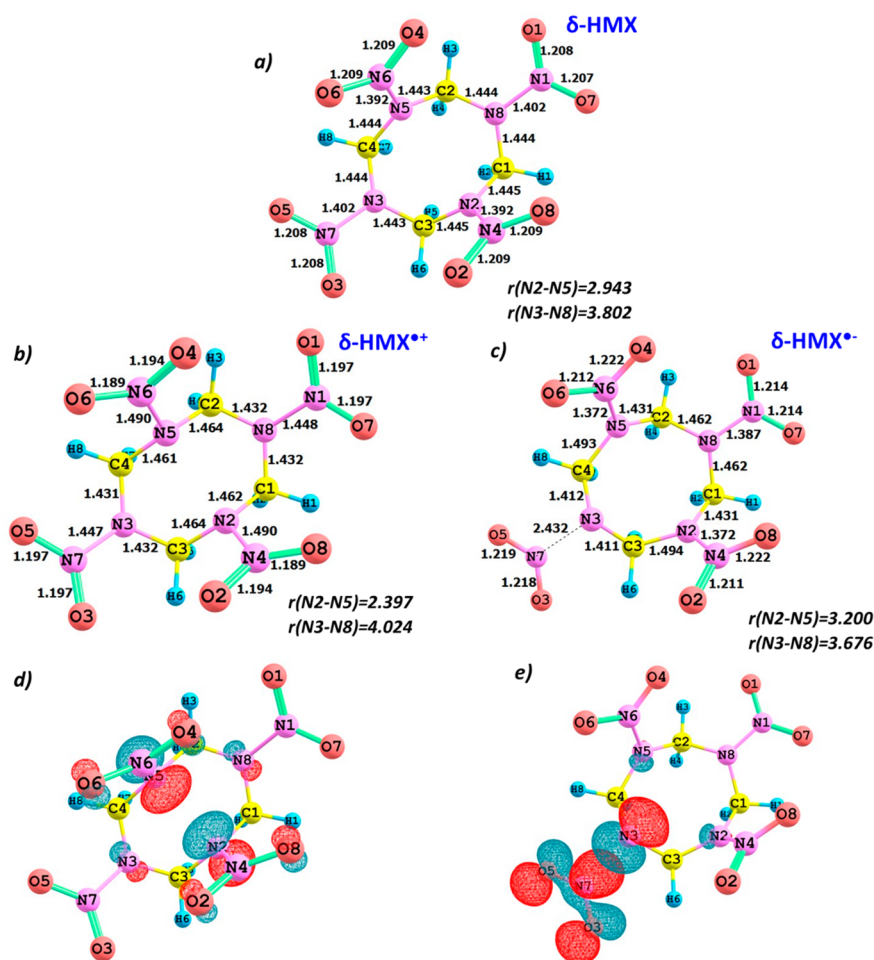
Figure 5. Optimized structures of (a) an equilibrium ground state δ-HMX molecule, (b) a δ-HMX radical cation (δ-HMX$^{\bullet+}$), and (c) a δ-HMX radical anion (δ-HMX$^{\bullet-}$). The bond lengths are in Å. Isosurfaces of (d) the hole (h^+) state in δ-HMX$^{\bullet+}$ and (e) the electron (e^-) state in δ-HMX$^{\bullet-}$.

Table 3. Reaction Activation Barriers, E (kcal/mol), Zero-Point Energy Corrected Barriers, E_{ZPE}, (kcal/mol), Reaction Energies (shown in parentheses), and Pre-Exponential Factors (lgA, s^{-1}) of the δ-HMX Ion Radical Decomposition Reactions

		M06			PBE	
reaction		E	E_{ZPE}	lgA	E	E_{ZPE}
Neutral δ-HMX Molecule						
1	δ-HMX $\rightarrow$ (CH$_2$N-NO$_2$)$_3$-CH$_2$N$^{\bullet}$ + $^{\bullet}$NO$_2$	50.8	45.5	18.6	45.1	40.3
Ionized δ-HMX$^{\bullet+}$ Ion Radical						
2	δ-HMX$^{\bullet+} \rightarrow$ [(CH$_2$N-NO$_2$)$_3$-CH$_2$N + NO$_2$]$^{\bullet+}$	32.5	–	–	30.4	–
3	δ-HMX$^{\bullet+} \rightarrow$ (CH$_2$N-NO$_2$)$_3$-CH$_2$N$^{\bullet}$ + NO$_2^+$	37.0	35.4	–	50.8	48.8
	$\mathbf{1}^{\bullet+} \rightarrow \mathbf{6}^{\bullet+}$, Fig 6 δ-HMX$^{\bullet+} \rightarrow$ (CH$_2$N)$_3$-(NO$_2$)$_2$-CHN-NO(OH)$^+$ + NO$_2^{\bullet}$	(−24.3)	(−26.6)	–	(−13.0)	(−15.1)
4	(a) HONO isomerization Fig 6, step $\mathbf{1}^{\bullet+} \rightarrow \mathbf{2}^{\bullet+}$ δ-HMX$^{\bullet+} \rightarrow$ (CH$_2$N-NO$_2$)$_3$-CHN-NO(OH)$^{\bullet+}$	12.7 (−8.6)	10.1 (−8.6)	13.4	13.0 (1.6)	10.1 (1.4)
	(b) step $\mathbf{4}^{\bullet+} \rightarrow \mathbf{5}^{\bullet+}$: (CH$_2$N-NO$_2$)$_3$-CHN-NO(OH)$^{\bullet+} \rightarrow$ (CH$_2$N)$_3$-(NO$_2$)$_2$-CHN-NO(OH)$^+$ +NO$_2^{\bullet}$	10.0 (0.8)	8.6 (−1.8)	13.4	–	–
5	step $\mathbf{1}^{\bullet+} \rightarrow \mathbf{8}^{\bullet+}$: (CH$_2$N-NO$_2$)$_3$-CHN-NO(OH)$^{\bullet+} \rightarrow$ (CH$_2$N)$_3$-(NO$_2$)$_3$-CHN$^{\bullet+}$ + HONO	(−13.6)	(−17.0)	–	–	–
	(a) step $\mathbf{7}^{\bullet+} \rightarrow \mathbf{8}^{\bullet+}$: (CH$_2$N-NO$_2$)$_3$-CHN-NO(OH)$^{\bullet+} \rightarrow$ (CH$_2$N)$_3$-(NO$_2$)$_3$-CHN$^{\bullet+}$ + HONO	12.4 (12.4)	11.2 (11.2)	–	–	–
Negatively Charged δ-HMX$^{\bullet-}$ Ion Radical						
6	δ-HMX$^{\bullet-} \rightarrow$ [(CH$_2$N-NO$_2$)$_3$-CH$_2$N + NO$_2$]$^{\bullet-}$	12.5	–	–	4.8	–
7	δ-HMX$^{\bullet-} \rightarrow$ (CH$_2$N-NO$_2$)$_3$-CH$_2$N$^-$ + NO$_2^{\bullet}$	17.0	15.4	15.8	9.0	7.6
8	δ-HMX$^{\bullet-} \rightarrow$ (CH$_2$N-NO$_2$)$_3$-CH$_2$N$^{\bullet}$ + NO$_2^-$	31.5	30.2	–	38.1	36.5

The optimized structure of δ-HMX$^{\bullet+}$ has a significantly narrower tetra-azaoctane ring (Figure 5) than the neutral molecule. This is a reflection of the N2−N5 interatomic distance being 0.6 Å shorter and the N3−N8 distance being 0.2 Å larger as compared to the neutral molecule. There are also minor changes, such as an increased N−NO$_2$ bond and a

shortened axial C−N bond (Figure 5). The lowest unoccupied molecular orbital with β-spin, corresponding to the hole (h^+) component of the ionized molecule, is mainly formed by 2p$_y$ atomic orbitals of N5 and N2 nitrogen atoms (Figure 5e).

In studying decomposition mechanisms, we probed two different reaction models of the N−NO$_2$ bond fission. In the
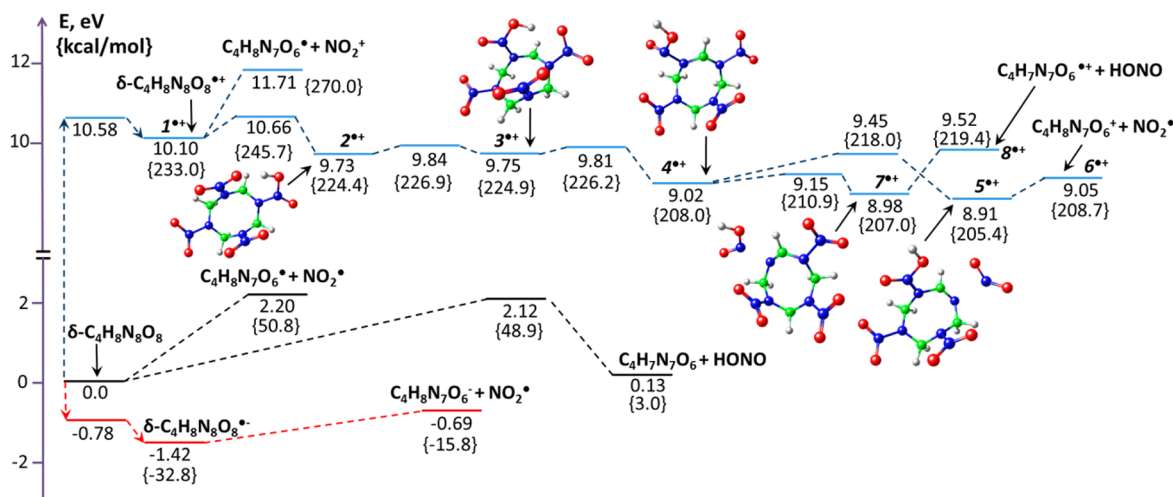
Figure 6. Energy diagram illustrates the gas-phase fragmentation pathways of the neutral and charged δ-HMX molecules. All numbers are obtained with M06 functional.
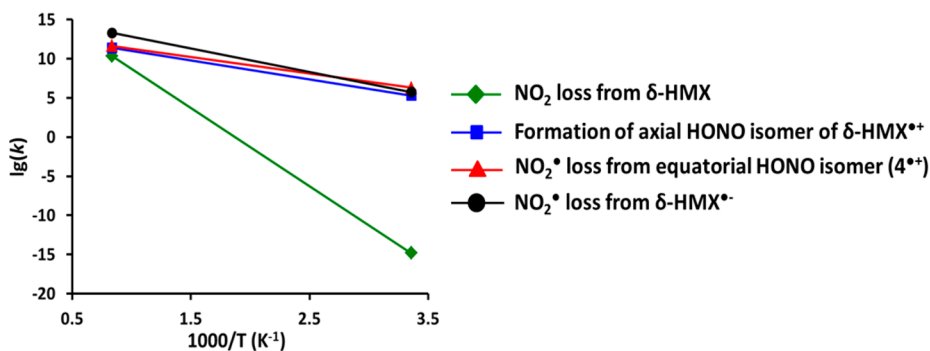

Figure 7. Reaction rates of the gas-phase molecular decomposition reactions of neutral and charged δ-HMX.

first model (referred hereafter as a split charge model), which asymptotically simulates a dissociation of a charged ion into two products, both of which share a positive charge (reaction 2, Table 3), the axial N−NO$_2$ bond distance of δ-HMX$^{\bullet+}$ was enlarged and fixed at 7.3 Å, keeping both chemically split products within the same physically calculated system.

The positive charge (a hole, h^+) in the system is distributed over both products regardless of how far from each other they are placed. The energy of such a process (the same as the activation barrier) is 32.5 kcal/mol (Table 3), which is ∼18 kcal/mol lower than the corresponding process in the neutral molecule (reaction 2, Table 3).

In the second model (referred hereafter as a localized charge model), which approximates a dissociation process with the hole fully localized on only one of the reaction products (reactions 3 and 4, Table 3), the reaction energy was obtained as a sum of the total energies of the separately calculated reaction products. The reaction 3 (Table 3) describes the formation of the isolated NO$_2^+$ cation and the neutral (CH$_2$N-NO$_2$)$_3$-CH$_2$N$^\bullet$ radical residue. The resultant activation energy of such a process is 37.0 kcal/mol (Figure 6, Table 3), which is 13 kcal/mol (when ZPE correction is included, see Table 3) lower than the energy of the corresponding reaction in the neutral molecule. As expected from simple electrostatic considerations and Table 2, the obtained total energy of the system with the hole well-localized on one of the completely isolated products is lower than that of the system in which the hole is delocalized over the separated products. In addition, in

accordance with Table 2, the hole favors localization on the residue (reaction 4, Table 3) over localization on NO$_2$ (reaction 3, Table 3) and even more so over splitting between both products. The lower barrier of the charge split between products in comparison to the charge localized on the nitro group (32.5 vs 37.0 kcal/mol, Table 3) is underestimated due to Coulomb repulsion of the positively charged products (and hence the overestimated total energy of the final system's state).

Naturally, the most interesting reactions of the δ-HMX$^{\bullet+}$ fragmentation are related to an intricate detachment of neutral NO$_2^\bullet$ (paths $1^{\bullet+} \rightarrow 6^{\bullet+}$, Figure 6) or HONO elimination ($1^{\bullet+} \rightarrow 8^{\bullet+}$, Figure 6), while the hole is trapped on the residue. We note that they proceed very differently than the NO$_2$ loss and HONO-splitting from the neutral molecule, and both reactions have a common rate-determining step, which is unusual. These stepwise exothermic reactions (Table 3 and Figure 6) include a formation of axial ($2^{\bullet+}$) and equatorial ($3^{\bullet+}$ and $4^{\bullet+}$) HONO isomers of δ-HMX$^{\bullet+}$.

The formation of the axial HONO isomer $2^{\bullet+}$ requires 12.7 kcal/mol (Table 3, Figure 6) and is the rate-determining step for both the stepwise detachment of NO$_2^\bullet$ ($1^{\bullet+} \rightarrow 6^{\bullet+}$) and the HONO elimination ($1^{\bullet+} \rightarrow 8^{\bullet+}$) from δ-HMX$^{\bullet+}$, as it is clearly seen from the potential energy diagram depicted in Figure 6. The activation barrier of the axial HONO isomerization is significantly (by ∼25 kcal/mol) lower than the reaction energy calculated for the decomposition of δ-HMX$^{\bullet+}$ on the NO$_2^+$ cation and the neutral (CH$_2$N-NO$_2$)$_3$-CH$_2$N$^\bullet$ radical residue

(37.0 kcal/mol, Figure 6, Table 3). The axial ($2^{\bullet+}$) and equatorial ($3^{\bullet+}$) isomers are predicted to lie ~8.5 kcal/mol (Figure 6) lower in energy than δ-HMX$^{\bullet+}$.

The data obtained here imply that the earliest reactions in the δ-HMX$^{\bullet+}$ decomposition are activated with the energy of 10.1 kcal/mol and that the reactions include both the NO_2 loss and the HONO elimination, which will likely to proceed simultaneously and exothermally, with the generated heat of 17 (reaction 5) or 26.6 (reaction 4) kcal/mol. It is needless to say that such a decomposition will proceed much more rapidly and aggressively than the process from the neutral molecule (see Figure 7).

We note that despite the activation barriers to decompose the δ-HMX$^{\bullet+}$ cation are lower than the corresponding dissociation processes of the neutral molecule and that some reactions are highly exothermic, a fairly high HMX IP should be taken into account (Table 2) as it lowers a probability for the reaction. Such a high IP protects the molecule from spontaneous breakdown and makes the decomposition from the positively charged state require effectively higher energy than decomposition from the neutral molecule. Nevertheless, the energetic considerations suggest that in the electron-deficient environment, the bond dissociation will be facilitated and will proceed faster than in a neutral molecule, releasing sufficiently large amount of heat.

Our calculations also demonstrate that the formation of HONO-isomers is possible only in the case of positively charged δ-HMX molecules and not for the neutral (see section 4.2) or the negatively charged δ-HMX (*fide infra*). Interestingly, a somewhat similar discrimination was observed in DADNE.[34] However, unlike HMX, it was found that the intramolecular hydrogen transfer leading to the HONO formation is precluded from the neutral and positively charged DADNE molecule, and only an electron-rich environment supports such a rearrangement.

4.2.2. Decomposition of δ-HMX$^{\bullet-}$. Due to its positive electron affinity, the δ-HMX readily traps an electron, forming δ-HMX$^{\bullet-}$, and gains energy in the process (Table 2). The molecular structure of the δ-HMX$^{\bullet-}$, anion radical (Figure 5), is characterized by an elongated N3−N7 bond by ~1 Å. The observed bond elongation appears coherent with the lengthened axial N−N bond of a β-HMX anion radical.[105] The δ-HMX$^{\bullet-}$ highest occupied orbital with α-spin has a shape of σ^* antibonding molecular orbital (Figure 5) and is predominately formed by $2p_x$ and $2p_y$ atomic functions of O3, O5 oxygen and N3, N7 nitrogen atoms.

In simulating the NO_2 loss from δ-HMX$^{\bullet-}$, we explored both the split charge and localized charge dissociation models with three possibilities for the resulting products: (i) both products are negative (calculated as two split products separated by 7.0 Å within the same calculation as described in reaction 6, Table 3); (ii) the $(CH_2N-NO_2)_3$-CH_2N^- residue is negative, and the NO_2 is neutral (calculated as two isolated products, described by reaction 7, Table 3); and (iii) the NO_2^- is negative, and the $(CH_2N-NO_2)_3$-CH_2N is neutral (also calculated as two isolated products, following reaction 8, Table 3). A comparison of electronic affinities of products (Table 2) should govern the preference between the three possibilities, hence the reaction that produces the fully localized electron on the residue should be most favorable. Indeed, Table 3 shows that the elimination of neutral $NO_2^\bullet$ (reaction 7, Table 3) requires 14.5 kcal/mol lower energy than the elimination of the negative NO_2^- (reaction 8, Table 3). Hence reaction 7, leaving an extra

electron on the $(CH_2N-NO_2)_3$-CH_2N residue, is most favorable.

All attempts to find alternative decomposition pathways of δ-HMX$^{\bullet-}$, such as the HONO elimination or NONO rearrangement, have failed. We were not able to find a stable product configuration or a well-defined transition state. Hence, excess of electrons favors the NO_2 loss and practically suppresses other decomposition routes. This is consistent with and explains the results of recent experimental studies, which considered the NO_2 moiety as the fingerprint for fragmentation of widely used nitro explosives such as HMX,[105] RDX[106] and PETN[107] under dissociative attachment electron experiments. Once again, the termination of some reaction channels imposed by the charge in δ-HMX radical echoes the similar trend observed in DADNE.[34]

Summarizing the ion radical calculations, we conclude that the ions of δ-HMX, both positively and negatively charged, require lower activation energies for the detachment of the NO_2 moiety than the neutral molecules. In other words, both an electron-rich and electron-deficient surroundings of the δ-HMX molecules would facilitate and accelerate the decomposition process. The IP is rather high, and therefore some additional energy is required to form the cation. However, once the cation is formed, very little additional energy is required to breakdown the system and the reaction becomes autocatalytic due to high exothermicity. With the trend of the molecule to quickly trap an electron due to its positive electron affinity, a large reduction of activation barriers was observed for δ-HMX radical anion with a clear trend to favor the NO_2 loss mechanism at expense of other possible channels, which become suppressed. Naturally, such a dramatic energy reduction also affects reaction rates. Figure 7 illustrates that the decomposition of ions proceeds at significantly higher rates than the decomposition of the neutral molecule despite lower pre-exponential factors (Table 3). Most importantly, excess of electrons (or holes) allows for an accurate control of chemical decomposition of δ-HMX radical ions and hence carries implications for developing sensor, detector, and ignition devices.

Important questions emerge, such as whether some conditions exist that create an electro-magnetic field within (or near) condensed materials (as opposed to charged isolated molecules) to trigger the explosive chemistry through other than the ground-state potential energy surfaces and whether the qualitative results obtained on ions would be replicated at the solid-state processes.

4.3. (001) Surface Decomposition. Our calculations of decomposition of the ideal bulk δ-HMX crystals only confirmed the tendencies observed on the neutral molecules, illustrated in Table 4. This is not at all surprising as both systems, the δ-HMX molecule and the molecular crystal, are neutral; they exhibit quite similar behavior with the already well-known trend

Table 4. Calculated Activation Barriers and Reaction Energies for δ-HMX Decomposition Reactions in Gaseous Phase and Ideal Bulk Are Given in kcal/mol[a]

	gas phase		ideal bulk crystal
reaction	M06	PBE	PBE
(i) NO_2 loss	50.8 (50.8)	45.1 (45.1)	50.8 (50.8)
(ii) HONO elimination	48.9 (3.0)	38.0 (0.7)	49.4 (−2.8)

[a]Energies do not include ZPE corrections.

Table 5. Calculated Activation Barriers of Decomposition Reactions from Charged States of δ-HMX Are Given in kcal/mol[a]

reaction	gas phase				(001) surface	
	cation		anion		positively charged	negatively charged
	M06	PBE	M06	PBE	PBE	PBE
(i) split charge NO$_2$ loss	32.5	30.4	12.5	4.8	34.5	9.4
(ii) NO$_2$ loss	12.7 (−24.3)	13.0 (−13.0)	17.0 (17.0)	9.0 (9.0)	~20.7 (−6.0)	20.1 (20.1)
(iii) HONO isomerization	12.7 (−8.6)	13.0 (1.6)	no reaction		~20.7 (12.9)	no reaction

[a]Reaction energies (no ZPE corrections included) are shown in parentheses.

of showing visibly higher activation barriers and somewhat longer reaction times in the condensed phase relative to the gas phase. We also note here that the kinetic parameters obtained here for δ-HMX reaffirm kinetics known for β-HMX and therefore do not offer any logical explanation for differences in sensitivities of those phases.

Here, we show that the dipole moment characteristic of polar δ-HMX generates a surface charge sufficiently large to trigger the explosive decomposition under a very small external perturbation.

Figure 2 shows the structure of δ-HMX with the identified (001) polar direction. Analyses of projected density of states and Bader charges indicate that the electric field generated by the molecular dipoles induces a *charge transfer* such that the "positive" surface has excess positive charge, 0.25 holes per molecule, and the "negative" surface has excess negative charge, 0.25 electrons per molecule (Figure 2). This quantitatively proves that the surface is polar and charged.

We focus now on how does the discovered (001) surface charge transfer[32,80] affects the δ-HMX decomposition kinetics and mechanisms. Here we simulated decomposition reactions on both positively and negatively charged (001) surfaces, including the cleavage of the axial N-NO$_2$ bond and the HONO isomerization as the two most kinetically favorable pathways.

4.3.1. Decomposition of the Positively Charged Surface. For reliable comparison and completeness we follow the similar computational strategy as was used for ion radicals, while bearing in mind the trends revealed from Table 2, which dictate that the neutral NO$_2$ (or HONO) should split off, leaving a positive charge localized on the surface residue. Hence, to calculate the energy of the NO$_2$ loss from the δ-HMX molecule on the (001) surface we again employed two types of calculations. In the split charge model, the axial N−NO$_2$ bond distance was enlarged and fixed at 5.0 Å. The energy of such a process is 34.5 kcal/mol (Table 5), which is comparable to the case of cation radical δ-HMX$^{\bullet+}$ and appreciably lower than the reaction barriers of neutral molecules in the gas phase (~45.1 kcal/mol, Table 4, see also Table 1) and in the crystal bulk (50.8 kcal/mol, Table 4).[80] Due to a very large supercell size we were not able to determine ZPE corrections, but we may assume that they would reduce the energy of N−N bond cleavage by another ~5 kcal/mol.

Owing to the complex reaction profile in addition to the oversized supercell, it is problematic to directly calculate all stages of the reaction pathway. Hence, to simulate these reactions, we calculated reaction energies and used a reasonable approximation to roughly estimate the activation barriers by using the geometry configurations of the transition states, obtained for decomposition of ions. The reaction energy, obtained from a sum of the total energies of the isolated neutral NO$_2$ and the positively charged (CH$_2$N-NO$_2$)$_3$-CH$_2$N$^{\bullet+}$

residue on the (001) surface, is found to be −6.0 kcal/mol. This is comparable to cation decomposition (−13.0 kcal/mol). Similarly to the molecular cation, the (CH$_2$N-NO$_2$)$_3$-CH$_2$N residue on the positively charged (001) surface tends to relax into the HONO isomer. An inspection of Bader charges confirms that the hole is completely localized on the axial HONO isomer. The estimated barrier of such a rearrangement is ~20.7 kcal/mol, also comparable to the cation (13.0 kcal/mol). The reaction energy of the axial HONO isomer formation is 12.9 kcal/mol (Table 5), which is somewhat higher than the reaction energy calculated for the corresponding reaction in δ-HMX$^{\bullet+}$ cation (1.6 kcal/mol).

Thus, the hole trapped on the polar δ-HMX surface has a pronounced effect on stability of the material. The simulated reactions, exothermic NO$_2$ loss and (endothermic) HONO-isomerization, generally proceed following a scenario closely resembling the cation decomposition. The corresponding activation barriers are significantly reduced relative to the neutral crystal bulk reaction and to the neutral gas-phase reaction.

4.3.2. Decomposition of the Negatively Charged Surface. The negatively charged (001) surface (Figure 2) also bears a strong effect on the axial N−N bond cleavage pathway. According to our calculations, the detachment of the axial NO$_2$ from δ-HMX, if it proceeds on the negatively charged surface, requires only 9.4 kcal/mol or lower[80] (Table 5), which is comparable with 4.8 kcal/mol (Table 5, see also Table 3) estimated for δ-HMX$^{\bullet-}$ within the same split charge model.

The localized charge model yields 20.1 kcal/mol (Table 5) for the reaction energy of the NO$_2$ loss which is somewhat higher than the corresponding anion reaction estimate (9.0 kcal/mol). Nevertheless, it is still significantly lower (by 25−30 kcal/mol) than the energy required for the detachment of NO$_2$ in the gas phase and bulk material (Tables 4 and 5). Once ZPE corrections are included, the resultant energy would be further reduced by another ~5 kcal/mol, reaching ~15 kcal/mol. At the same time, the extra electron precludes the surface from decomposition through the HONO isomerization channel, showing the discrimination parallel to the anion processes (Table 5). Interestingly, the low activation barriers obtained here indicate a rather high sensitivity of δ-HMX to thermal initiation. The estimated barriers (~15−21 kcal/mol) are far lower than 32−35 kcal/mol obtained for the sensitivity benchmark compound PETN,[41] the most sensitive secondary high explosive in its class; all materials that exhibit higher sensitivity than PETN are classified as primary explosives. For example, heavy metal azides, SrN$_6$, CuN$_3$, PbN$_6$, and AgN$_3$, representatives of primary explosives, exhibit barriers of 20, 27, 29, and 32 kcal/mol, respectively.[108] Thus, while β-HMX is a typical secondary explosive, the δ-polymorph is not.

Most importantly, δ-HMX crystals exhibit comparable behavior at both negatively and positively charged surfaces

with the decomposition triggered by a relatively modest perturbation and proceeding very rapidly, initiating a violent explosive reaction.

The conclusions obtained here have vast consequences. First of all, a logical explanation of differences in sensitivity of β-HMX and δ-HMX phases to initiation of detonation can be now proposed. Interactions of molecular dipoles generate the polarization-induced charge separation, which prompts the polar surfaces of the δ-HMX crystals to decompose much faster than nonpolar grains of the β-HMX crystals. Second of all, the wide range of experimental activation barriers reported for HMX can be attributed to various crystallographic phases, including both β- and δ-HMX. With polar δ-HMX facets requiring appreciably lower activation energy than β-HMX facets, an unusually large scattering of activation barriers in the overall thermal initiation should be expected. The scattered energy interval, in fact, makes a lot of sense if one recalls that the experimental data (e.g., in mass spectroscopy and DSC and TGA measurements) strongly depend on the heating rate, especially taking into account that the β-to-δ phase transition's energy also falls into the same range. In other words, relative fractions of β- and δ-HMX phases in the decomposing material, most likely, vary in experiments. Thus, a lower end of the reported interval, 13 to 25−35 kcal/mol, which was previously regarded as erroneous results,[52,62] may be actually associated with a degradation of the polar δ-HMX surfaces. The medium range of 40−46 kcal/mol in energy is related to decomposition of the nonpolar β-phase surfaces, and the higher energies, above 46 kcal/mol, are probably relevant to other processes or system components, for example, evaporated molecules, plastic binders, or other additives. Third of all, the understanding gained here reveals a clear correlation between the presence of polar surfaces and decomposition kinetics, which can be used to adjust sensitivity of the high explosive material to detonation by choosing certain crystallographic polymorphs. This is illustrated by the fact that the sensitivity of δ-HMX is high, comparable to primary explosives, and the sensitivity of β-HMX is relatively low, comparable to other secondary explosives. Such a manipulation of a materials' composition and morphology makes it possible to fine-tune the surface chemistry for targeted applications.

5. SUMMARY AND CONCLUSION

In this study, the earliest stages of possible chemical decomposition reactions of δ-HMX were simulated by means of quantum-chemical methods in a range of state-of-the-art DFT approximations. The decomposing molecules were placed in various environments to represent a model system with an increasing level of complexity, making a transition from an idealized isolated molecule or an ion to condensed materials. A comparative analysis included the single gas-phase neutral molecules in their ground state (δ-HMX), ionized molecule (δ-HMX$^{\bullet+}$), negatively charged ion (δ-HMX$^{\bullet-}$), and molecules placed in an ideal bulk crystal and on a (001) crystal surface.

We found that the molecular decomposition process of δ-HMX from its ground state hardly differs from β-HMX as the obtained activation barriers, dissociation mechanisms, pre-exponential factors, and reaction rates in both molecules are quite similar. Knowing that δ-HMX is visibly more sensitive that β-HMX, this observation leads us to conclude that the intramolecular interactions that were modified due to the change of the molecular conformation from the δ-HMX (boat)

structure to the β-HMX (chair) structure barely contribute to the sensitivity of those materials.

Next, we simulated the decomposition of radical ions of δ-HMX and discovered that both the cation and anion require notably less energy to trigger decomposition than the neutral molecule. This implies that once the molecule is placed in polarized surroundings (such as electron- or hole- excess conditions), the reaction will be triggered with a very small additional energy and progress rapidly.

Further, we compared the major decomposition pathways in ideal bulk crystals of δ-HMX and β-HMX. The reaction parameters were again fairly similar to each other[32] and to their neutral molecular analogs. Thus, it may appear as if intermolecular interactions, which are certainly different in the two perfect crystals, also failed to provide any explanation of different sensitivities between polymorphs. The seeming contradiction is lifted if one recalls that chemistry of materials studied in experiments differs from perfect bulk model crystals that were explored in our study. Specifically, it is nowadays well-established that decomposition reactions do not start in the middle of densely packed ideal bulk crystals and only molecules placed next to defects or deformations exhibit activation barriers that are consistent with the observed in experiments.[32,109]

Furthermore, simulations of decomposition pathways of δ-HMX molecules placed on the (001) surface demonstrated that the polar surface causes holes (h^+) and electrons ($e-$) to separate, which, in turn, creates favorable conditions for initiation of a fast reaction. Indeed, the activation barrier for NO_2 loss in the hole-rich or electron-rich environment is significantly reduced, implying that the reaction will be triggered with a modest perturbation, significantly smaller than that required to ignite β-HMX and will proceed very rapidly. Interestingly, both electron excess and electron deficit will catalyze the fast reaction. We predict that the presence of holes triggers simultaneous decomposition via the NO_2 loss and HONO elimination channels, which proceed through the same rate-determining step. The presence of electrons clearly favors the NO_2 loss pathway and effectively suppresses other channels. The major difference between δ-HMX and β-HMX chemistries is defined by fundamental differences in properties of chemically active polar δ-HMX surfaces versus relatively more passive nonpolar β-HMX surfaces. We predict that the decomposition chemistry of β-HMX would also be facilitated in the presence of an additional charge; however, adding this charge to the system will require some additional external energy. The polar (001) surfaces of δ-HMX naturally create such conditions by polarizing the surface and separating holes and electrons, which triggers fast chemistry, with no additional energy needed.

While a correlation between a polar axis and accelerated reaction rates in organic crystals was reported earlier (see, for example, refs 42 and 43), the δ-HMX decomposition mechanisms, scrutinized here, unravel a great deal of detail on how the surface polarization considerably affects the surface chemistry. Those results offered a logical explanation for different sensitivity of δ-HMX and β-HMX polymorphs to detonation initiation. Our conclusions also removed long-standing contradictions and explained a large set of measurements reported a strangely wide range of experimental values of thermal decomposition of HMX.

In conclusion, the formation of crystals possessing a polar direction, a property shown by many common organic and

inorganic materials, is one of the most remarkable aspects of solid-state chemistry. The crystallographic polarization played an extremely important role, for example, in inspiring the recognition of the relationship between optical activity and molecular structure and in the first resolution of an organic compound by Pasteur. Although the stereochemistry of organic crystals became more widespread and there is increased awareness of the common occurrence of polar organic crystals and their great structural diversity, specific knowledge of chemical and physical behavior of those materials is still limited, and therefore the potential utility of their unique properties is not fully realized. The understanding gained in this study of the structure of polymorphs of organic molecular crystals and the principles governing their crystal packing and their chemical reactivity is instrumental in a more rapid development of methods to control surface and interface chemistry. The resulting control of surface reactions will not only provide the means of causing them when they are desired, for example, for catalysis or synthesis of targeted materials but also the means of preventing them when they are to be avoided, as in stabilization of pharmaceuticals or elimination of accidental explosions and fires.

■ ASSOCIATED CONTENT

Ⓢ Supporting Information

The structures of nitro molecules, structures of products and transition states of gas-phase δ-HMX decomposition pathways, the structures of reaction intermediates and transition states of the $NO_2^{\bullet}$ and HONO detachment reactions from δ-HMX$^{\bullet+}$, and absolute energies and the coordinates of the atoms in all the molecules whose geometries were optimized. This material is available free of charge via the Internet at http://pubs.acs.org.

■ AUTHOR INFORMATION

Corresponding Author
mkukla@nsf.gov; mkukla@umd.edu
Notes
The authors declare no competing financial interest.

■ ACKNOWLEDGMENTS

■ REFERENCES

(1) Bowden, F. P.; McAuslan, J. *Nature* **1956**, *178*, 408−410.
(2) Bowden, F. P.; Montagu-Pollock, H. M. *Nature* **1961**, *191*, 556−559.
(3) Reed, E. J.; Manaa, M. R.; Fried, L. E.; Glaesemann, K. R.; Joannopoulos, J. D. *Nat. Phys.* **2008**, *4*, 72−76.
(4) Fried, L. E.; Manaa, M. R.; Pagoria, P. F.; Simpson, R. L. *Annu. Rev. Mater. Res.* **2001**, *31*, 291−321.
(5) Bowden, F. P.; Mulcahy, M. F. R.; Vines, R. G.; Yoffe, A. *Proc. R. Soc.* **1947**, *188*, 291−311.
(6) Robertson, A. J. B.; Yoffe, A. *Nature* **1948**, *161*, 806−807.
(7) Kuklja, M. M.; Stefanovich, E. V.; Kunz, A. B. *J. Chem. Phys.* **2000**, *112*, 3417−3423.
(8) Kuklja, M. M. *Appl. Phys. A: Mater. Sci. Process.* **2003**, *76*, 359−366.
(9) Liu, W. G.; Zybin, S. V.; Dasgupta, S.; Klapötke, T. M.; Goddard, W. A., III *J. Am. Chem. Soc.* **2009**, *131*, 7490−7491.
(10) Furman, D.; Kosloff, R.; Dubnikova, F.; Zybin, S. V.; Goddard, W. A., III; Rom, N.; Hirshberg, B.; Zeiri, Y. *J. Am. Chem. Soc.* **2014**, *136*, 4192−4200.
(11) Sharia, O.; Kuklja, M. M. *J. Am. Chem. Soc.* **2012**, *134*, 11815−11820.
(12) Tarver, C. M. *J. Phys. Chem. A* **1997**, *101*, 4845−4851.
(13) Bernstein, E. R. *Adv. Quantum Chem.* **2014**, *69*, 31−71.
(14) Williams, F. *Adv. Chem. Phys.* **1971**, *21*, 289−302.
(15) Dremin, A. N. *Chem. Phys. Reports* **1995**, *14*, 1851−1870.
(16) Dremin, A. N. *Towards detonation theory*; Springer-Verlag: New York, 1999 pp 156.
(17) Yu, Z.; Bernstein, E. R. *J. Chem. Phys.* **2011**, *135*, 154305−154305−10.
(18) Aluker, E. D.; Krechetov, A. G.; Mitrofanov, A. Yu; Nurmukhametov, D. R.; Kuklja, M. M. *J. Phys. Chem. C* **2011**, *115*, 6893−6901.
(19) Owens, F. J.; Sharma, J. *J. Appl. Phys.* **1980**, *51*, 1494−1497.
(20) Sharma, J.; Beard, B. C. In Structure and Properties of Energetic Materials. Proceedings of the MRS Symposium, Boston, MA, November 30−December 2, 1992; Liedenberg, D. H., Armstrong, R. W., Gilman, J. J.., Eds.; MRS: Pittsburgh, PA, 1993.
(21) Duval, G. E. In *Shock Waves in Condensed Matter*; Gupta, Y. M., Eds; Plenum Press: New York, 1985.
(22) Gilman, J. J. *Science* **1996**, *247*, 65.
(23) Aduev, B. P.; Aluker, E. D.; Belokurov, G. M.; Krechetov, A. G. *Chem. Phys. Rep.* **1997**, *16*, 1479−1485; *Chem. Phys. Rep.* **1998**, *17*, 469.
(24) Kuklja, M. M.; Aduev, B. P.; Aluker, E. D.; Krasheninin, V. I.; Krechetov, A. G.; Mitrofanov, A. Yu. *J. Appl. Phys.* **2001**, *89*, 4156−4166.
(25) Kunz, A. B.; Kuklja, M. M.; Botcher, T. R.; Russel, T. P. *Thermochim. Acta* **2002**, *384*, 279−284.
(26) Aluker, E. D.; Krechetov, A. G.; Mitrofanov, A. Y.; Zverev, A. S.; Kuklja, M. M. *J. Phys. Chem. C* **2012**, *116*, 24482.
(27) Kunz, A. B. *Phys. Rev. B* **1996**, *53*, 9733−9738.
(28) Kunz, A. B. *Mater. Res. Soc. Symp. Proc.* **1996**, *418*, 287−292.
(29) Kuklja, M. M.; Kunz, A. B. *J. Phys. Chem. Solids* **2000**, *61*, 35−44.
(30) Kuklja, M. M.; Kunz, A. B. *J. Appl. Phys.* **1999**, *86*, 4428−4434.
(31) Kuklja, M. M.; Kunz, A. B. *J. Phys. Chem. B* **1999**, *103*, 8427−8431.
(32) Kuklja, M. M. *Adv. Quantum Chem.* **2014**, *69*, 71−146.
(33) Aluker, E. D.; Krechetov, A. G.; Mitrofanov, A. Y.; Zverev, A. S.; Kuklja, M. M. *Molecules* **2013**, *18*, 14148−14160.
(34) Kimmel, A. V.; Sushko, P. V.; Shluger, A. L.; Kuklja, M. M. *J. Chem. Phys.* **2007**, *126*, 234711−234711−10.
(35) Aluker, E. D.; Aluker, N. L.; Krechetov, A. G.; Mitrofanov, A. Y.; Nurmuhametov, D. R.; Shvayko, V. N. *Russ. J. Phys. Chem. B* **2011**, *5*, 67−74.
(36) Guo, Y. Q.; Bhattacharya, A.; Bernstein, E. R. *J. Chem. Phys.* **2008**, *128*, 034303.
(37) Yu, Z.; Bernstein, E. R. *J. Phys. Chem. A* **2013**, *117*, 1756−1764.
(38) Sharia, O.; M. M. Kuklja, M. M. *J. Phys. Chem. A* **2010**, *114*, 12656−12661.
(39) Sharia, O.; M. M. Kuklja, M. M. *J. Phys. Chem. B* **2011**, *115*, 12677−12686.
(40) Sharia, O.; M. M. Kuklja, M. M. *J. Phys. Chem. C* **2012**, *116*, 11077−11081.
(41) Tsyshevsky, R. V.; Shaaria, O.; Kuklja, M. M. *J. Phys. Chem. C* **2013**, *117*, 18144−18153.
(42) Paul, I. C.; Curtin, D. Y. *Science* **1975**, *187.4171*, 19−26.
(43) Curtin, D. Y.; Paul, I. C. *Chem. Rev.* **1981**, *81*, 528−541.
(44) Noguera, C. *J. Phys.: Condens. Matter* **2000**, *12*, R367−R410.
(45) Noguera, C. *Physics and Chemistry at Oxide Surfaces*; Cambridge University Press: Cambridge, 1996.
(46) Goniakowski, J.; Finocchi, F.; Noguera, C. *Rep. Prog. Phys.* **2008**, *71* (016501), 55.
(47) Tarver, C. M.; Tran, T. D. *Combust. Flame* **2004**, *137*, 50−62.

(48) Cady, H. H.; Larson, A. C.; Cromer, D. T. *Acta Crystallogr. B* **1963**, *16*, 617−623.

(49) Choi, C. S.; Boutin, H. P. *Acta Crystallogr. B* **1970**, *26*, 1235−1240.

(50) Main, P.; Cobbledick, R. E.; Small, R. W. H. *Acta Crystallogr. C* **1985**, *41*, 1351−1354.

(51) Cobbledick, R. E.; Small, R. W. H. *Acta Crystallogr. B* **1974**, *30*, 1918−1922.

(52) Brill, T. B.; Karpowicz, R. J. *J. Phys. Chem.* **1982**, *86*, 4260−65.

(53) Karpowicz, R. J.; Brill, T. B. *Appl. Spectrosc.* **1983**, *37*, 79−81.

(54) Henson, B. F.; Asay, B. W.; Sander, R. K.; Son, S. F.; Robinson, J. M.; Dickson, P. M. *Phys. Rev. Lett.* **1999**, *82*, 1213−1216.

(55) Henson, B. F.; Smilowitz, L.; Asay, B. W.; Dickson, P. M. *J. Chem. Phys.* **2002**, *117*, 3780−3788.

(56) Henson, B. F.; Smilowitz, L.; Asay, B. W.; Dickson, P. M. *J. Chem. Phys.* **2002**, *117*, 3789−3798.

(57) Surber, E.; Lozano, A.; Lagutchev, A.; Kim, H.; Dlott, D. D. *J. Phys. Chem. C* **2007**, *111*, 2235−2241.

(58) Herrmann, M.; Engel, W.; Eisenreich, N. *Propellants, Explos., Pyrotech.* **1992**, *17*, 190−195.

(59) Asay, B. W.; Henson, B. F.; Smilowitz, L. B.; Dickson, P. M. *J. Energetic Mater.* **2003**, *21*, 223−235.

(60) Urtiew, P. A.; Forbes, J. W.; Tarver, C. M.; Vandersall, K. S.; Garcia, F.; Greenwood, D. W.; Hsu, P. C.; Maienschein, J. L. *AIP Conf. Proc.* **2004**, *706*, 1053−1056.

(61) Brill, T. B.; Reese, C. O. *J. Phys. Chem.* **1980**, *84*, 1376−1380.

(62) Brill, T. B.; Gongwer, P. E.; Williams, G. K. *J. Phys. Chem.* **1994**, *98*, 12242−12247.

(63) Chakraborty, D.; Muller, R. P.; Dasgupta, S.; Goddard, W. A., III. *J. Phys. Chem. A* **2001**, *105*, 1302−1314.

(64) Glascoe, E. A.; Hsu, P. C.; Springer, H. K.; DeHaven, M. R.; Tan, N.; Turner, H. C. *Thermochim. Acta* **2011**, *515*, 58−66.

(65) Kimura, J.; Kubota, N. *Propellants Explos. Pyrotech* **1980**, *5*, 1−8.

(66) Whelan, D. J.; Mark R. F. A Reassessment of the Kinetics of the Thermal Decomposition of the High Explosive, Delta-HMX, in the Range 508 to 524 K, as Studied by Isothermal Gravimetry. *NASA Database*, 19980218798; NASA: Washington, DC, 1998.

(67) Bulusu, S.; Weinstein, D. I.; Autera, J. R.; Velicky, R. W. *J. Phys. Chem.* **1986**, *90*, 4121−4126.

(68) Hohenberg, P.; Kohn, W. *Phys. Rev.* **1964**, *136*, B864−B71.

(69) Kohn, W.; Sham, L. J. *Phys. Rev. A* **1965**, *140*, A1133−A38.

(70) Perdew, J. P.; Burke, K.; Ernzerhof, M. *Phys. Rev. Lett.* **1996**, *77*, 3865−3868.

(71) Adamo, C.; Barone, V. *J. Chem. Phys.* **1999**, *110*, 6158−6169.

(72) Chai, J.-D.; Head-Gordon, M. *Phys. Chem. Chem. Phys.* **2008**, *10*, 6615−6620.

(73) Frisch, M. J.; Trucks, G. W.; Schlegel, H. B.; Scuseria, G. E.; Robb, M. A.; Cheeseman, J. R.; Scalmani, G.; Barone, V.; Mennucci, B.; Petersson, G. A.; Nakatsuji, H.; Caricato, M.; Li, X.; Hratchian, H. P.; Izmaylov, A. F.; Bloino, J.; Zheng, G.; Sonnenberg, J. L.; Hada, M.; Ehara, M.; Toyota, K.; Fukuda, R.; Hasegawa, J.; Ishida, M.; Nakajima, T.; Honda, Y.; Kitao, O.; Nakai, H.; Vreven, T.; Montgomery, J. A., Jr.; Peralta, J. E.; Ogliaro, F.; Bearpark, M.; Heyd, J. J.; Brothers, E.; Kudin, K. N.; Staroverov, V. N.; Kobayashi, R.; Normand, J.; Raghavachari, K.; Rendell, A.; Burant, J. C.; Iyengar, S. S.; Tomasi, J.; Cossi, M.; Rega, N.; Millam, M. J.; Klene, M.; Knox, J. E.; Cross, J. B.; Bakken, V.; Adamo, C.; Jaramillo, J.; Gomperts, R.; Stratmann, R. E.; Yazyev, O.; Austin, A. J.; Cammi, R.; Pomelli, C.; Ochterski, J. W.; Martin, R. L.; Morokuma, K.; Zakrzewski, V. G.; Voth, G. A.; Salvador, P.; Dannenberg, J. J.; Dapprich, S.; Daniels, A. D.; Farkas, Ö.; Foresman, J. B.; Ortiz, J. V.; Cioslowski, J.; Fox, D. J. *Gaussian 09*, revision B.01; Gaussian, Inc.: Wallingford, CT, 2009.

(74) Zhao, Y.; Truhlar, D. G. *Acc. Chem. Res.* **2008**, *41*, 157−167.

(75) Zhao, Y.; Truhlar, D. G. *Theor. Chem. Acc.* **2008**, *120*, 215−241.

(76) Blöchl, P. E. *Phys. Rev. B* **1994**, *50*, 17953−17979.

(77) Kresese, G.; Futhmuller, J. *Comput. Mater. Sci.* **1996**, *6*, 15−50.

(78) Kresse, G.; Furthmuller, J. *Phys. Rev. B* **1996**, *54*, 11169−11186.

(79) Kresse, G.; Hafner, J. *Phys. Rev. B* **1993**, *47*, RC558−561.

(80) Sharia, O.; Tsyshevsky, R.; Kuklja, M. M. *J. Phys. Chem. Lett.* **2013**, *4*, 730−734. The preliminary calculations reported in this Letter were performed in a 16-molecule supercell, which possess a dipole moment. Coulomb interactions of the dipole-induced electromagnetic field and the charged reaction products may lead to overestimated activation barriers. The present study refines the decomposition mechanisms by using the doubled, 32-molecule supercell with zero dipole moment. This change however causes only a small variation in numbers and does not skew the general qualitative conclusions obtained in both studies.

(81) Henkelman, G.; Uberuaga, B. P.; Jónsson, H. *J. Chem. Phys.* **2000**, *113*, 9901−9904.

(82) Hratchian, H. P.; Schlegel, H. B. *J. Chem. Phys.* **2004**, *120*, 9918−24.

(83) Hratchian, H. P.; Schlegel, H. B. *J. Chem. Theory Comput.* **2005**, *1*, 61−69.

(84) Hanggi, P.; Talkner, P.; Borkovec, M. *Rev. Mod. Phys.* **1990**, *62*, 251−341.

(85) Truhlar, D. G.; Garrett, B. C. *Annu. Rev. Phys. Chem.* **1984**, *35*, 159−189.

(86) Tang, W.; Sanville, E.; Henkelman, G. *J. Phys.: Condens. Matter* **2009**, *21*, 084204−1−7.

(87) Sanville, E.; Kenny, S. D.; Smith, R.; Henkelman, G. *J. Comput. Chem.* **2007**, *28*, 899−908.

(88) Henkelman, G.; Arnaldsson, A.; Jónsson, H. *Comput. Mater. Sci.* **2006**, *36*, 254−360.

(89) Oyumi, Y.; Brill, T. B. *Combust. Flame* **1985**, *62*, 213−224.

(90) Sadhukhan, S.; Muñoz, D.; Adamo, C.; Scuseria, G. E. *Chem. Phys. Lett.* **1999**, *306*, 83−87.

(91) Nachimuthu, S.; Gao, J.; Truhlar, D. G. *Chem. Phys.* **2012**, *400*, 8−12.

(92) Tsyshevsky, R. V.; Kuklja, M. M. *Molecules* **2013**, *18*, 8500−8517.

(93) Zhang, S.; Truong, T. N. *J. Phys. Chem. A* **2000**, *104*, 7304−7307.

(94) Chavez, D. E.; Hanson, S. K.; Veauthier, J. M.; Parrish, D. A. *Angew. Chem.* **2013**, *125*, 7014−7017.

(95) Joas, M.; Klapötke, T. M.; Szimhardt, N. *Eur. J. Inorg. Chem.* **2014**, *2014*, 493−498.

(96) Lifshitz, C.; Rejwan, M.; Levin, I.; Peres, T. *Int. J. Mass Spectrom. Ion Process* **1988**, *84*, 271−282.

(97) White, M. G.; Colton, R. J.; Lee, T. H.; Rabalais, J. W. *Chem. Phys.* **1975**, *8*, 391−398.

(98) Lias, S. G.; Levin, R. D.; Kafafi, S. A. Ion Energetics Data. In *NIST Chemistry WebBook, NIST Standard Reference Database Number 69*; Linstrom, P. J., Mallard, W. G., Eds.; National Institute of Standards and Technology, Gaithersburg, MD; http://webbook.nist.gov (accessed June 20, 2014).

(99) Dewar, M. J. S.; Shanshal, M.; Worley, S. D. *J. Am. Chem. Soc.* **1969**, *91*, 3590−3594.

(100) Kimura, K.; Katsumata, S.; Achiba, Y.; Yamazaki, T.; Iwata, S. Ionization energies, Ab initio assignments, and valence electronic structure for 200 molecules. In *Handbook of HeI Photoelectron Spectra of Fundamental Organic Compounds*; Japan Scientific Society Press: Tokyo, Japan, 1981.

(101) Koo, L. K.; Chin, W. S.; Mok, C. Y.; Huang, H. H. *Bull. Singapore Natl. Inst. Chem.* **1990**, *18*, 121.

(102) Katsumata, S.; Shiromaru, H.; Mitani, K.; Iwata, S.; Kimura, K. *Chem. Phys.* **1982**, *69*, 423−431.

(103) Clemmer, D. E.; Armentrout, P. B. *J. Chem. Phys.* **1992**, *97*, 2451.

(104) Ervin, K. M.; Ho, J.; Lineberger, W. C. *J. Phys. Chem.* **1988**, *92*, 5405−5412.

(105) Postler, J.; Goulart, M. M.; Matias, C.; Mauracher, A.; da Silva, F. F.; Scheier, P.; Limão-Vieira, P.; Denifl, S. *J. Am. Soc. Mass. Spectrom.* **2013**, *24*, 744−752.

(106) Sulzer, P.; Mauracher, A.; da Silva, F. F.; Denifl, S.; Märk, T. D.; Probst, M.; Limão-Vieira, P.; Scheier, P. *J. Chem. Phys.* **2009**, *131*, 144304−1−234711−7.

(107) Edtbauer, A.; Sulzer, P.; Mauracher, A.; Mitterdorfer, C.; Ferreira da Silva, F.; Denifl, S.; Märk, T. D.; Probst, M.; Nunes, Y.; Limão-Vieira, P.; Scheier, P. *J. Chem. Phys.* **2010**, *132*, 134305−1−134305−8.

(108) Fox, P. G.; Hutchinson, R. W. Slow thermal decomposition. In *Energetic Materials, Physics and Chemistry of Inorganic Azides*; Fair, H. D., Walker, R. F., Eds.; Plenum Press: New York and London, 1977; pp 255.

(109) Kuklja, M. M. *J. Phys. Chem. B* **2001**, *105*, 10159−10162.

13302

dx.doi.org/10.1021/ja506297e | *J. Am. Chem. Soc.* 2014, 136, 13289−13302